COMPUTER VISION AND IMAGE UNDERSTANDING
Vol. 62, No. 3, November, pp. 382–391, 1995

Skeletonization via Distance Maps and Level Sets

RON KIMMEL, DORON SHAKED, AND NAHUM KIRYATI

Electrical Engineering Department, Technion, Haifa 32000, Israel

AND

ALFRED M. BRUCKSTEIN

Computer Science Department, Technion, Haifa 32000, Israel

Received September 6, 1994; accepted November 7, 1994

The medial axis transform (MAT) of a shape, better known as its skeleton, is frequently used in shape analysis and related areas. In this paper a new approach for determining the skeleton of an object is presented. The boundary is segmented at points of maximal positive curvature and a distance map from each of the segments is calculated. The skeleton is then located by applying simple rules to the zero sets of distance map differences. A framework is proposed for numerical approximation of distance maps that is consistent with the continuous case and hence does not suffer from digitization bias due to metrication errors of the implementation on the grid. Subpixel accuracy in distance map calculation is obtained by using gray-level information along the boundary of the shape in the numerical scheme. The accuracy of the resulting efficient skeletonization algorithm is demonstrated by several examples. © 1995 Academic Press, Inc.

1. INTRODUCTION

In this paper we present a new approach to shape skeletonization. The importance of the skeleton, or medial axis, was discussed by Blum in [6, 7] with motivation from visual perception analysis. Mathematical properties of the medial axis transform (MAT) has been investigated over the years in many papers starting with [21, 22] and are still of great interest to the computer vision community [23, 34, 4]. Skeletons are frequently used as shape descriptors, e.g., in character recognition.

In [21] Montanari gives four (equivalent) definitions for the skeleton of shapes in the real plane. The first is the prairie fire model, the skeleton points being the locations where the propagating wavefront initiated on the shape boundary "intersects itself." This model of wavefront propagation uses the Hüygens principle and shock capturing as in optics and fluid dynamics. The boundary propagates with a constant velocity along its normal direction and the skeleton points are the shocks that appear during the propagation. Shocks are the collisions of "ignition lines" [28], as seen in Fig. 1a. The propagating wavefront carries information about the boundary. Thus, using the prairie fire point of view, the skeleton points may be regarded as points in which shape boundary information vanishes. The second approach defines the skeleton as the set of "ridges" on the distance map surface measured from the boundary; see Fig. 1b. The third model considers the skeleton as the geometric location of centers of maximal disks. A *maximal disk* is a disk contained in the shape, for which there exists no other disk in the shape that contains it; see Fig. 1c. The last model defines a skeleton as the set of points that do not belong to any straight line segment connecting other points to their respective closest boundary points; see Fig. 1d.

The four definitions mentioned above motivated a wealth of discrete implementations on binary images over the last two decades [1, 2, 9, 16, 19]. A skeletonization approach that has recently gained attention is the use of the Voronoi diagrams, e.g., [5, 23, 32].

Roughly speaking, the skeletonization algorithms may be divided into three classes. Most algorithms operate on binary pixel images [1, 2, 9, 16, 19]. Other algorithms operate on polygons that are assumed to be provided by some polygonal approximation of the boundary [3, 15, 21]. Only few algorithms try to deal with the general problem of skeletonization for smooth shapes [11, 30]. The algorithm proposed in this paper belongs to all three classes. Motivated by global properties of the boundary and skeleton curves, we present a discrete implementation that is consistent with the continuous case.

In principle, each skeleton point corresponds to at least two boundary points. Those points are the boundary points

1077-3142/95 $12.00

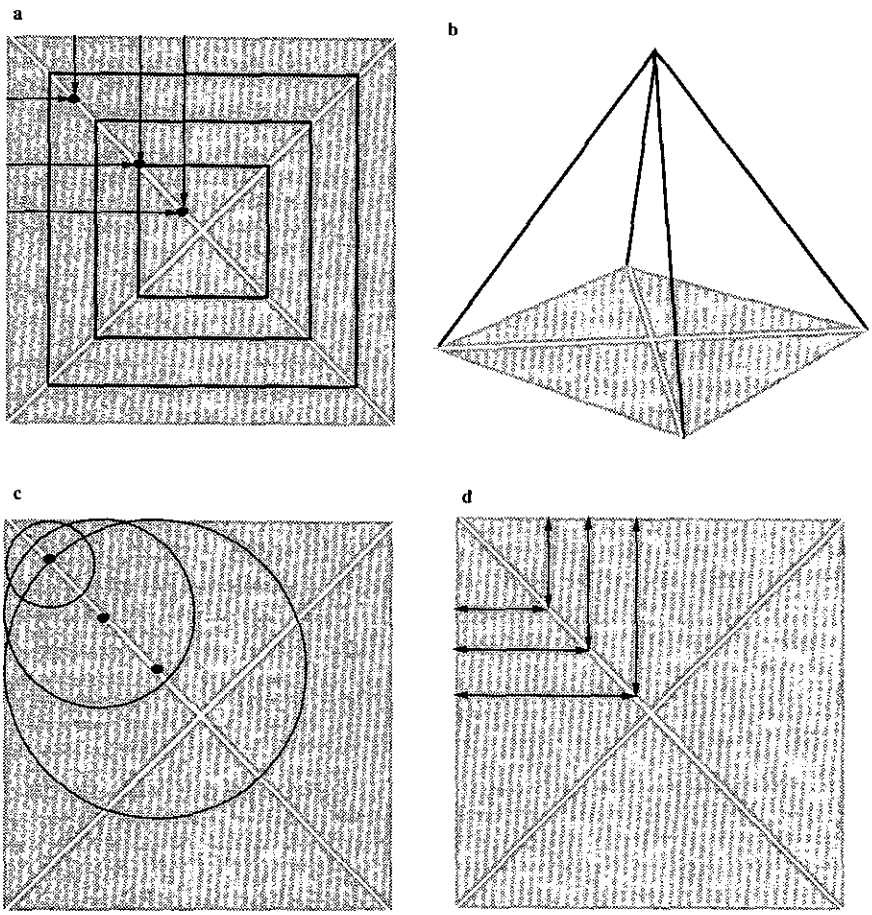

FIG. 1. Illustration of the four points of view on the skeleton (white) of an object (gray). (a) The black curves are offsets of the boundary obtained by constant velocity propagation. The set of shocks (self-intersection points) of the propagating curves generate the skeleton. The arrows from the boundary to skeleton points represent ignition lines. (b) The skeleton is the planar projection of the ridges of the distance map from the boundary. The ridges are shown as black curves in 3-D, where the third dimension represents distance. (c) The skeleton is the set of centers of maximal disks. (d) The skeleton is considered as the set of points that do not belong to any straight line connecting other interior points to their respective closest boundary points.

with Hüygens wavefronts that met at the skeleton point, or alternatively, the boundary points touching the maximal disk centered on the skeleton point. The skeleton point is located at the intersection of the normals to the two boundary points, and the distances between the skeleton point and both boundary points are equal. Therefore, if we segment the boundary into small segments and find a distance map from each of those segments, the skeleton will be located at places where at least two distance maps share the same value. Those locations could be equivalently defined as zero sets of distance map differences.

The above description is based on the implicit assumption that we know how to segment the boundary so that no pair of boundary points corresponding to the same skeleton point belong to the same segment. This would be trivially accomplished by a very fine boundary segmentation which would lead to high computational complexity. Indeed, if we segment the boundary at each boundary pixel, we arrive at Voronoi-diagram-based skeletonization [18, 5, 23].

In order to solve the boundary segmentation problem, we study the relation between positive curvature maxima along the boundary and the skeleton. In particular, we show that a skeleton point is never generated by a single curve segment defined between successive positive curvature maxima. The symmetry–curvature duality was previously explored by Leyton in [17]. In [25] that duality was used in constructing the "curvature skeleton" of binary images.

The structure of this paper is as follows: In Section 2 we present the skeletonization algorithm for the continuous (preimage) case. A discrete approximation of the proposed algorithm is introduced in Section 3, employing gray-level information along the boundary to find the curvature along an implicit subpixel representation of the object boundary. Examples of applying the algorithm to image data are

presented in Section 4. In the Appendix we state and prove a version of the Four Vertex Theorem [10]. It is used in Section 2 to prove the correctness of the skeletonization algorithm construction.

2. THE SKELETON AND CURVATURE MAXIMA

Let the boundary of an object be given by a simple closed planar curve $\mathscr{C}(s) \in \mathbb{R}^2$, where s is the arclength parameterization along the curve. The curvature $\kappa(s)$ is defined [10, 31] as the magnitude of the second derivative of the curve with respect to its arclength, a positive sign being assigned at convex points and a negative sign at concave points.

As explained in the introduction, a skeleton point generally corresponds to at least two boundary points that touch the maximal disk. We refer to those points as the boundary points "generating" the skeleton point. In order to justify our new skeletonization approach we prove the following property of the skeleton–boundary relation.

THEOREM 1. *A boundary segment connecting two points that generate a skeleton point contains at least one internal point having a positive curvature maximum.*

Proof. Given a boundary segment connecting two points that generate a skeleton point, the maximal disk corresponding to the skeleton point is tangent to the boundary at the end points of the boundary segment. Those two points segment the disk boundary into two circular segments. Consider a new shape defined by the boundary segment and the "outer" or opposite circle segment of the maximal disk. We now apply a version of the well-known Four Vertex Theorem [10], which is stated and proven in the Appendix. According to the Four Vertex Theorem, the boundary of the new shape has at least two distinct points at which the curvature is both positive and locally maximal. The circle segment on the boundary may account for only one such point. The other has to be found within the segment of the original boundary. ∎

This theorem provides the basis for the required boundary segmentation

COROLLARY 1. *If we segment the shape boundary at points of positive maximal curvature, points generating its skeleton always belong to different boundary segments.*

An algorithm for skeletonization follows from this result. Its outline is:

1. Find the curvature along the boundary curve and split the boundary into segments at points of maximal positive curvature. The arclength parameters of the segmentation points, are referred to by s_i, where $i \in \{0, 1, \ldots, N-1\}$, $(s_N \equiv s_0)$. N being the number of local positive curvature maxima.

FIG. 2. The white hole in the black object has a boundary segment along which the total curvature is less than -2π.

2. For each segment calculate the Euclidean distance map over the whole image domain $\Omega \subseteq \mathbb{R}^2$. For the ith segment of the boundary curve, $\mathscr{C}(s) : s \in [s_i, s_{i+1}]$, the distance map $\mathscr{D}_i : (x, y) \in \Omega \to \mathbb{R}^+$, is defined as

$$\mathscr{D}_i(x, y) = \inf_{s \in [s_i, s_i+1]} \{d(\mathscr{C}(s), (x, y))\},$$

where $d(p, q)$ is the Euclidean distance between the two points p and q.

3. Find a preliminary skeleton as the location of the zero-level sets of all distance map differences.

$$\hat{\mathscr{S}} = \{(x, y) : \forall i, j; i \neq j, (\mathscr{D}_i - \mathscr{D}_j = 0) \cap (\cap_{k \neq i,j} \mathscr{D}_i < \mathscr{D}_k)\}, \tag{1}$$

where $i, j, k \in \{0, 1, \ldots, N-1\}$. $\hat{\mathscr{S}}$ is clearly the Voronoi diagram of the curve segments.

4. Eliminate all exterior points (background points), and all points located on branches starting at points $\mathscr{C}(s_i)$ with a distance from $\mathscr{C}(s_i)$ less than $1/\kappa(s_i)$. The elimination process is performed sequentially starting with the branch corresponding to the largest curvature maximum and ending with the smallest positive curvature maximum. False branches corresponding to larger curvature maxima are deleted first so that they will not interfere with the deletion process of false branches corresponding to smaller curvature maxima that are connected to them.

Note that for the segmentation of a closed curve, we need to assign at least two partition points. Assigning a partition point at points of positive maximal curvature results in a legal segmentation of the boundary, due to the Four Vertex Theorem, which ensures the existence of at least two such points.

The skeletonization algorithm described above operates well on all shapes unless they have a specifically shaped hole in them; see Fig. 2. The reason for this problem is that the Four Vertex Theorem does not apply to boundaries of holes in shapes, or in other words, a shape (the shape of the hole) does not necessarily have two boundary points

with *negative* curvature minima. However, if a shape has a single negative curvature minimum, the boundary necessarily contains a convex segment with a tangent turn angle that is larger than 2π; see Fig. 2. Therefore, to make this algorithm general, we add an arbitrary segmentation point to every hole boundary with a turn angle less than -2π.

In the next section a discrete version of the algorithm is devised. Gray-level information along the object boundary is used to achieve subpixel accuracy in the numerical implementation.

3. DISCRETE APPROXIMATION

The numerical approximation used for implementing the proposed skeletonization algorithm considers the gray-level information at the pixels along the object boundary for interpolating the boundary curve and its corresponding curvature. One possible model of the relation between the image pixels and the continuous preimage describes the object boundary between the grid points by first thresholding the object from the background and then interpolating the boundary between the pixels. We shall consider the boundary to be a level set of the image gray-level function, or alternatively, without loss of generality, we may consider the boundary to be the zero-level set of the gray level minus a given threshold, as in [13]. We also assume a local linear behavior of the gray-level function near that zero set. The planar curvature of any level set $f^{-1}(\mathbf{c})$, where $\mathbf{c}$ stands for a constant, of the function $f: \mathbb{R}^2 \to \mathbb{R}$ is given by [10]

$$\kappa = \frac{f_{xx}f_y^2 - 2f_xf_yf_{xy} + f_{yy}f_x^2}{(f_x^2 + f_y^2)^{3/2}}. \tag{2}$$

First, the location of the boundary is obtained by linear interpolation (see [29] for a useful method for finding the boundary at a cell between four neighboring pixels). The curvature of the boundary at its intersections with the grid lines is then obtained by linear interpolation of the radius of curvature of level sets that pass through the two nearest grid points. Consider for example a grid line parallel to the x axis. Let the gray level at pixel i be $f_i \equiv f(i\Delta x) < 0$ and the gray level at the next pixel be $f_{i+1} > 0$. Then the zero set is interpolated to be at $\Delta x(i + |f_i|/(f_{i+1} - f_i))$, where Δx is the distance between the pixels. It is possible to calculate κ_i, the curvature of the f_i level set at pixel i using the simple central difference approximation for the partial derivatives in (2). The curvature at the zero crossing is interpolated as follows. For $\kappa_i\kappa_{i+1} > 0$, linear relation of the radius of curvature between successive level sets can be assumed and κ at the zero crossing is interpolated by

$$\kappa = \frac{|f_i| + |f_{i+1}|}{|f_{i+1}|\kappa_i^{-1} + |f_i|\kappa_{i+1}^{-1}}. \tag{3a}$$

If $\kappa_i\kappa_{i+1} < 0$ interpolation of the curvature itself at the zero crossing is more appropriate,

$$\kappa = \frac{|f_i|\kappa_i + |f_{i+1}|\kappa_{i+1}}{|f_{i+1}| + |f_i|}. \tag{3b}$$

The above scheme provides the curvature values at the intersection points of the boundary and the grid lines.

Now the local positive maxima of the curvature can be detected and used for boundary segmentation. For each boundary segment the distance map is calculated. Two alternative techniques for computing subpixel distance maps in a way that is consistent with the continuous case are presented in [13] and in [14, 33]. Both methods use the gray-level information near the boundary as initial conditions. Since the image is not binarized, the subpixel boundary information that is implicitly contained in the gray levels is preserved. Having computed the N distance maps, the zero-level sets of the distance map differences yield the preliminary skeleton points (Eq. (1)).

The examples in the next section show synthetic objects created by first generating a binary image and then performing geometric smoothing to simulate the integration effect of a CCD. Some smoothing is usually necessary even with real gray-level images in order to reduce the effects of noise in the boundary on the skeleton. The geometric smoothing we used considers each gray-level set as a curve and propagates all the level sets simultaneously using a geometric heat flow [27]. The Osher–Sethian algorithm [24] for curvature-based flows is the basis for the numerical implementation of

$$\frac{\partial f}{\partial t} = |\nabla f|\kappa, \tag{4}$$

where κ is the curvature defined at each level set of the gray-level image f as in Eq. (2). The above differential equation was numerically implemented using central difference approximation in space and forward difference approximation in time.

Consider a certain level set to be given as a parameterized curve $\mathscr{C}(s) : [0, L] \to \mathbb{R}^2$, where s is the arclength parameterization of $\mathscr{C}$. If f evolves under (4), then $\mathscr{C}$, embedded as a level set in f, propagates in time according to

$$\mathscr{C}_t = \mathscr{C}_{ss},$$

or equivalently

$$\mathscr{C}_t = \kappa\vec{n},$$

where $\vec{n}$ is the unit normal to the curve $\mathscr{C}$.

We smooth the boundary by propagating the image f

according to Eq. (4) with $\Delta t \simeq \Delta x$. Next, the curvature is interpolated between the grid points along the linearly interpolated boundary, via Eq. (3). If there is more than one connected component like in the case of holes in the object or several objects, several curvature lists are generated. For each of the curvature lists, the curvature function is first smoothed using a moving average rectangular window. Then, local positive maxima are detected using a finite window on the curvature function. Both the moving average window and the local-maxima-detection window are used to eliminate noise effects.

In step 2 of the algorithm the boundary was segmented at points of local positive curvature maxima. Gray-level values in a 4-pixel-width envelope around each segment are then used as initial conditions for the distance map calculation procedure. For computing the distance from each segment, we used the iterative procedure of [12, 14, 33]. That procedure is a special case of the shape from shading algorithm of Rouy and Tourin [26]. In the continuous domain, let $\mathcal{D}_0 : \Omega(\subset \mathbb{R}^2) \to \mathbb{R}^+$ be equal to the gray-level values in an envelope $\mathcal{N} \subset \Omega$ along the given segment and $+\infty$ elsewhere, $\Omega \backslash \mathcal{N}$. The distance map of the segment is calculated by

$$\mathcal{D}_t = 1 - |\nabla \mathcal{D}|,$$

for $\mathcal{D} \in \Omega \backslash \mathcal{N}$. The following differential approximation of the above equation was proven in [26] to converge to the proper solution (in our case the distance map). Using the discrete notation $\mathcal{D}_{i,j}^N = \mathcal{D}(N\Delta t, i\Delta x, j\Delta y)$, first define

$$a \equiv D_-^x \mathcal{D}_{i,j} = (\mathcal{D}_{i,j} - \mathcal{D}_{i-1,j})/\Delta x$$

$$b \equiv D_+^x \mathcal{D}_{i,j} = (\mathcal{D}_{i+1,j} - \mathcal{D}_{i,j})/\Delta x$$

$$c \equiv D_-^y \mathcal{D}_{i,j} = (\mathcal{D}_{i,j} - \mathcal{D}_{i,j-1})/\Delta y$$

$$d \equiv D_+^y \mathcal{D}_{i,j} = (\mathcal{D}_{i,j+1} - \mathcal{D}_{i,j})/\Delta y.$$

Then, the following numerical scheme is used to update $\mathcal{D}$.

$$\mathcal{D}_{i,j}^{N+1} = \mathcal{D}_{i,j}^N - \Delta t(\sqrt{\max[(a^+)^2, (b^-)^2] + \max[(c^+)^2, (d^-)^2]} - 1),$$

where, $\alpha^+ \equiv \max(\alpha, 0)$ and $\alpha^- \equiv \min(\alpha, 0)$. The L^1 norm of the change between two successive iterations is used to set the stopping condition; see [33, 26].

The distance map from each segment and the values of the local positive curvature at the segments edges are used to produce the final skeleton. Subpixel accuracy is achieved by interpolating the skeleton between the grid points, making use of the values of the distance maps at each grid point. It is possible to handle junctions separately and to correct the "cutting" effect.

4. EXAMPLES

We have presented an algorithm for locating the skeleton of a given object in a picture with subpixel accuracy. A geometric property relating the local positive curvature maxima along the boundary and the skeleton points was presented. It is the basis for boundary segmentation that ensures that a skeleton point may not be generated by two points on the same boundary segment. The boundary segments were used to construct the skeleton via zero sets of distance map differences. The suggested algorithm readily lends itself to parallelization. The following examples demonstrate the operation of the algorithm.

Consider the object shown (after geometric smoothing) at the upper left frame in Fig. 3. The interpolated smoothed curvature along the outer and inner boundaries of the object are shown in the upper right frame. The lower left frame shows the pixels that correspond to the Voronoi diagram (before pruning). The branches to be pruned are the light gray pixel chains from the positive local curvature maxima along the boundary. The skeleton, interpolated to subpixel accuracy, is shown in the lower right frame. Additional objects and their skeletons are presented in Figs. 4, 5, and 6.

APPENDIX

In this appendix we state and prove a version of the well-known Four Vertex Theorem [10] using "skeleton terminology."

A circle may touch a curve at a single point or at several points. It may also coincide with the curve on an arc segment (or on several arc segments). We say that a disk touches a curve at two *separate points* p and q, if p and q do not belong to the same arc segment on which the disk boundary and the curve coincide.

In the sequel we use a few basic facts about the relation of a curve segment to disks touching it at a point p [8]. To avoid repetitions, we refer only to disks with centers located on the left side of the curve (the side to which the normal of convex segments point).

1. The curve penetrates all disks, touching it at p, unless they are tangent to the curve.
2. The centers of all tangent disks are located on the normal to the curve.
3. If the curvature of the curve at p is negative, then there exists a neighborhood of p in which the curve is outside all the disks tangent to it.
4. If the radius of a tangent disk is smaller than the radius of curvature of the curve at p, then there exists a neighborhood of p in which the curve is outside the disk. Note that the radius of curvature of a curve is $1/\kappa$, where κ is the curvature of the curve.
5. For convex curve segments, if the radius of a tangent

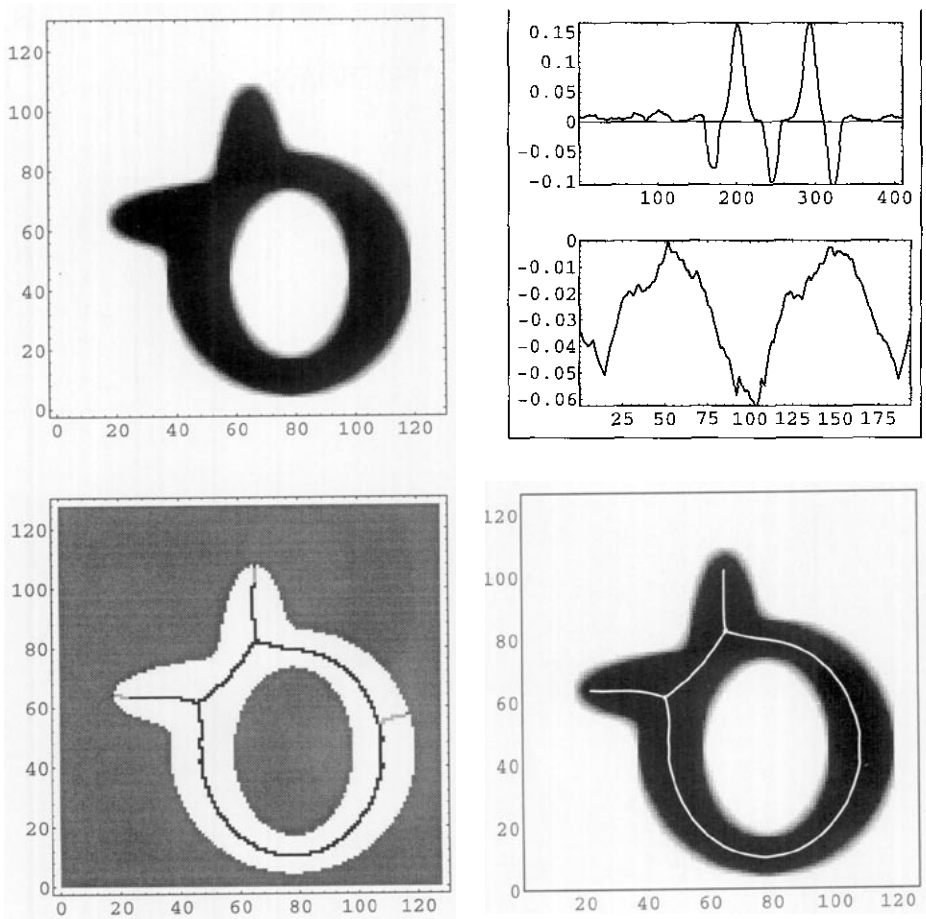

FIG. 3. (Upper left) An object after geometric smoothing. (Upper right) Interpolated curvature function along the outer boundary (upper graph) and inner boundary (lower graph). (Lower left) Voronoi diagram of the segments (preliminary skeleton) in which the branches to be pruned are in light gray. (Lower right) The skeleton is the white curve, interpolated to subpixel accuracy, shown on the object.

disk is larger than the radius of curvature of the curve at p, then there exists a neighborhood of p in which the curve is inside the disk.

6. For convex curve segments, if the radius of a tangent disk is equal to the radius of curvature of the curve at p, i.e., the disk is osculating the curve, then

(a) if the curvature of the curve at p is locally minimal, then there exists a neighborhood of p in which the curve is inside the disk.

(b) if the curvature of the curve at p is locally maximal, then there exists a neighborhood of p in which the curve is outside the disk.

(c) if the curvature of the curve at p is not extremal, then the curve penetrates the disk at p.

We conclude that for convex curve segments, if we inspect all disks tangent to the curve at a points p in order of increasing radii, the location of curve points in the neighborhood of p is initially outside of the disk and finally inside the disk. The change occurs when the radius of the disk is equal to the radius of curvature of the curve at p. At the change, the relation between the disk and the curve points in the neighborhood of p depends on the third-order behavior of the curve according to Fact 6 above.

LEMMA 1. *A maximal disk in a shape touches the shape in one of the following:*

1. *two or more separate points.*
2. *a single point or segment with a curvature that is positive and locally maximal.*

Proof. A maximal disk in a shape has to touch its boundary in at least one point, let us denote it by p. From Fact 1, it is clear that it has to be tangent to the boundary. Let us inspect the set of disks tangent to the boundary at p in order of increasing radii. Note that every tangent disk contains all the former tangent disks. Therefore, there may be only one maximal disk tangent to the boundary at p. The maximal disk is the first tangent disk for which either:

1. there is a boundary point, different from p, for which all larger disks contain external points in its neighborhood, or

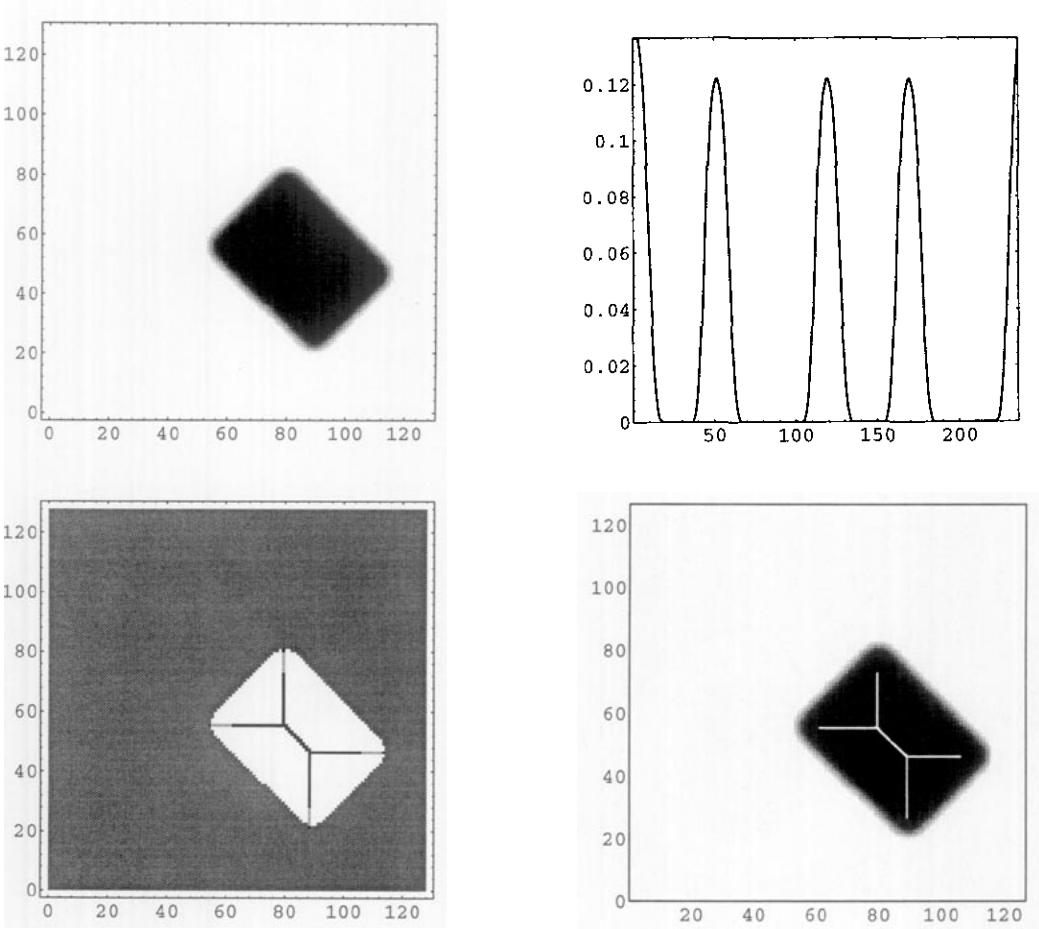

FIG. 4. (Upper left) A tilted "box"-object after geometric smoothing. (Upper right) Interpolated curvature function along the boundary. (Lower left) Voronoi diagram of the segments (preliminary skeleton) in which the branches to be pruned are in light gray. (Lower right) The skeleton is the white curve, interpolated to subpixel accuracy, shown on the object.

2. all larger disks contain external points in the neighborhood of p.

Case 1 above is clearly Case 1 of the lemma. From Fact 6 it is apparent that Case 2 may occur only at boundary points in which the curvature is positive and locally maximal. Case 2 is therefore Case 2 of the lemma. Note also that in those cases the radius of the maximal disk is equal to the radius of curvature of the boundary. ■

LEMMA 2. *Let $\overline{AB}$ and $\overline{CD}$ be two line segments in the plane, intersecting at a point E. Then, either $B \in C_C^D$ or $D \in C_A^B$, where C_A^B denotes the circle centered at A and passing through B and C_C^D denotes the circle centered at C and passing through D.*

Proof. We have to show (see Fig. 7), that either $BC \leq CD$ or $DA \leq AB$. Suppose the contrary is true, i.e., $BC > CD$ and $DA > AB$. Adding the two inequalities we get $BC + DA > CD + AB = CE + ED + AE + EB = (CE + EB) + (DE + EA)$ in contradiction to the triangle inequality $BC \leq CE + EB$ and $DA \leq DE + EA$. ■

COROLLARY 2. *Line segments connecting centers of maximal disks in a shape with their respective generating points on the boundary cannot intersect.*

If two such line segments intersect, at least one of the generating points is inside the other circle. Since the generating points are boundary points this other circle cannot be a maximal disk.

Given a shape and a maximal disk that touches it in two separate points p and q, we define two new shapes as follows: p and q define two arc segments on the maximal disk, and two respective boundary segments. The two new shapes are defined each by a boundary segment and the opposite arc segment, see Fig. 8.

LEMMA 3. *Both skeletons of the two new shapes include the center of the maximal disk, and their union is the skeleton of the full shape.*

Proof. We refer to the definition of the skeleton as the set of shocks of the propagating boundary, or the Prairie Fire Model. In the Prairie Fire Model a boundary point

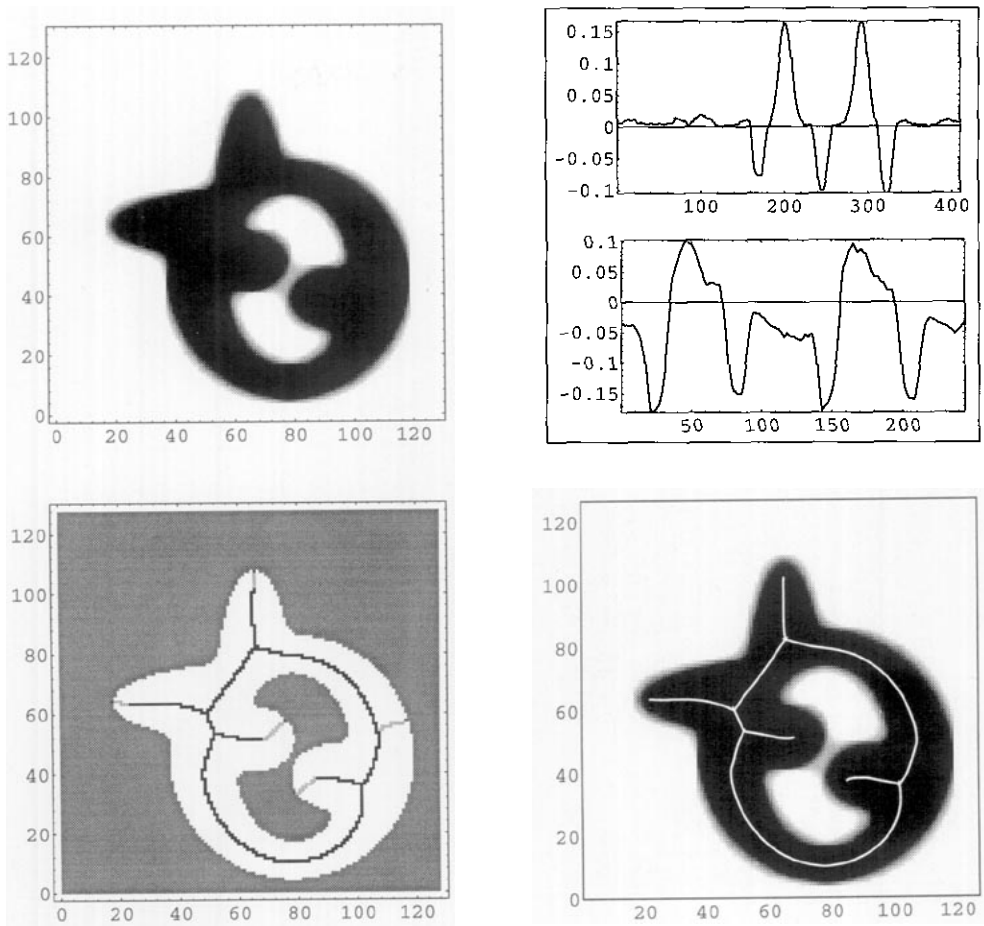

FIG. 5. (Upper left) An object after geometric smoothing. (Upper right) Interpolated curvature function along the outer boundary (upper graph) and inner boundary (lower graph). (Lower left) Voronoi diagram of the segments (preliminary skeleton) in which the branches to be pruned are in light gray. (Lower right) The skeleton is the white curve, interpolated to subpixel accuracy, shown on the object.

gets quenched at some skeleton point, as it meets another propagating boundary point. We will show that all skeleton points of the full shape belong to one of the new shapes and that no new skeleton point is due to the union. The essential statements are:

1. The propagation of all the points of the maximal disk segments in the new shapes meet at the center of the maximal disk.
2. All quenching pairs from the full shape quench each other in the new shapes (on points of the original skeleton).

Let us prove the first statement: All points propagating from the arc segments quench each other at the center of the original maximal disk. Assume by contradiction that a propagating arc segment point p_0 meets another propagating boundary point before it meets any other propagating arc segment point. This implies that the maximal disk touching point p_0 in the new shape has a smaller radius than the maximal disk. This cannot happen, since any such disk is contained in the maximal disk, which is contained in both new shapes.

We now show that pairs of generating points on the boundary of the full shape cannot be separated into different new shapes. Assume by contradiction that two points that generated a skeleton point of the full shape are each located on the boundary of a different new shape. In that case the radius connecting one of those points with the skeleton point corresponding to it must intersect one of the radii connecting the center of the maximal disk to either p or q, contradicting Corollary 2. Points p and q are the points generating the original maximal disk, see Fig. 8.

To prove the second statement we must show that in the new shapes, each boundary point is quenched by its original twin from the full shape. This is so since otherwise it must be quenched by another point from the boundary of the new shape. But this is impossible, it will not be quenched by another point that belongs to the full shape since it did not happen in the full shape in the first place; it

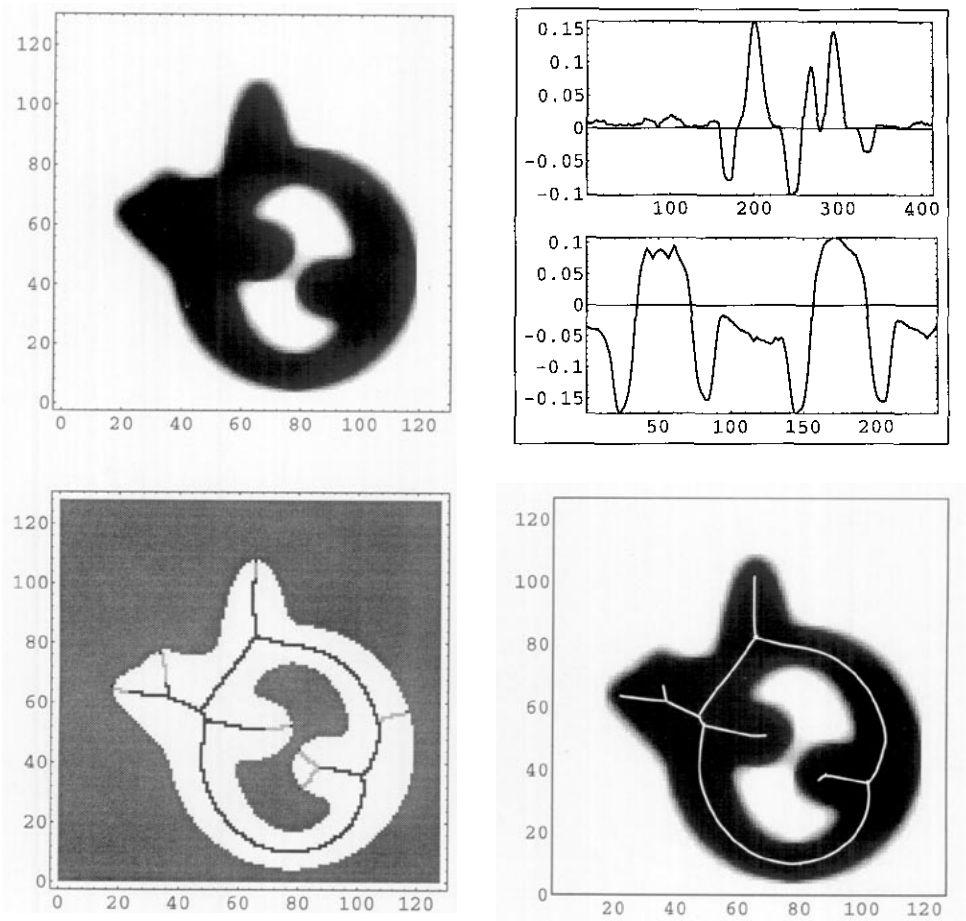

FIG. 6. (Upper left) An object after geometric smoothing. (Upper right) Interpolated curvature function along the outer boundary (upper graph) and inner boundary (lower graph). (Lower left) Voronoi diagram of the segments (preliminary skeleton) in which the branches to be pruned are in light gray. (Lower right) The skeleton is the white curve, interpolated to subpixel accuracy, shown on the object.

will not be quenched by a point from the newly introduced circular segments, since we have shown that all the arc segment points are quenched together. ■

The following corollary is a direct consequence of Lemma 3.

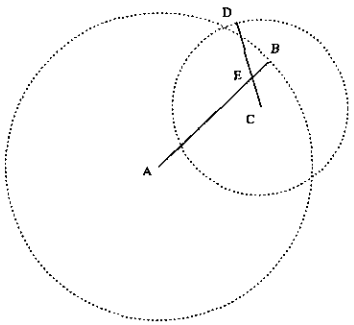

FIG. 7. Proof of Lemma 2.

COROLLARY 3. *The center of a maximal disk that touches the boundary in two separate points connects two different parts of the skeleton.*

The two parts are the skeletons of the two new shapes. Note that none of those parts is degenerate (i.e., a single point), since a single-point skeleton corresponds only to a circle. If one of the new shapes is a circle, the two boundary points are not separate points.

LEMMA 4. *An end point of the skeleton corresponds to a single boundary point with a curvature that is positive and locally maximal.*

Proof. From Lemma 1, it is sufficient to show that if a maximal disk is tangent to the boundary at two or more separate points, its center is not on an end point of the skeleton. This in turn is shown by Corollary 3. ■

THEOREM 2 (A VERSION OF THE FOUR VERTEX THEOREM [10]). *Every simply connected shape that is not a circle,*

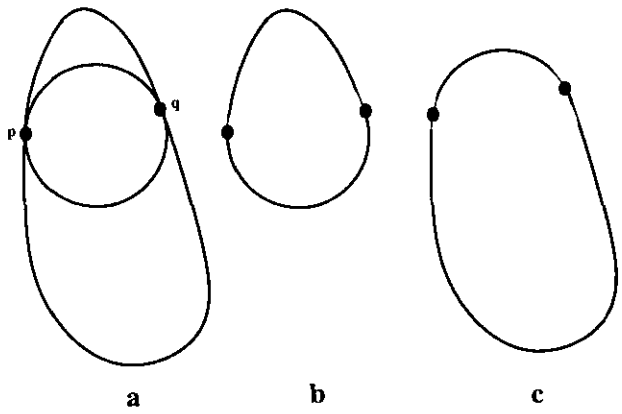

FIG. 8. Using the maximal disk it is possible to split the full shape into two new shapes.

has at least two boundary points in which the curvature is both positive and locally maximal.

Proof. Every simply connected shape has a simply connected skeleton [20]. Only circles have skeletons that are single points. Therefore, the skeletons of all other simply connected shapes have at least two end points. The proof follows immediately from Lemma 4. ■

ACKNOWLEDGMENTS

We thank Dr. Guillermo Sapiro for many helpful discussions on skeletons and distance transforms. This research was supported in part by the Ollendorf Center of the Department of Electrical Engineering, by the Technion VPR Funds, and by the Fund for the Promotion of Research at Technion.

REFERENCES

1. C. Arcelli, Pattern thinning by contour tracing, *CGIP* **17,** 1981, 130–144.
2. C. Arcelli and G. Sanniti di Baja, A width independent fast thinning algorithm, *IEEE Trans. PAMI* **7,** 1985, 463–474.
3. F. L. Bookstein, The line skeleton, *CGIP* **11,** 1979, 123–137.
4. J. W. Brandt, Convergence and continuity criteria for discrete approximations of the continuous planar skeleton, *CVGIP: Image Understanding* **59,** 1994, 116–124.
5. J. W. Brandt and V. R. Algazi, Continuous skeleton computation by Voronoi diagram, *CVGIP: Image Understanding* **55,** 1992, 329–338.
6. H. Blum, A transformation for extracting new descriptors of shape, in *Models for the Perception of Speech and Visual Form* (Walthen Dunn, Ed.), pp. 362–380, MIT Press, Cambridge, MA, 1967.
7. H. Blum, Biological shape and visual science (part I), *J. Theor. Biol.* **38,** 1973, 205–287.
8. J. W. Bruce and P. J. Giblin, *Curves and Singularities,* 2nd ed., Cambridge Univ. Press, Cambridge, UK 1992.
9. P. Danielson, Euclidean distance mapping, *CVGIP: Graphic Models Image Process.* **14,** 1980, 227–248.
10. M. P. Do Carmo, *Differential Geometry of Curves and Surfaces,* Prentice Hall, NJ, 1976.
11. P. J. Giblin and S. A. Brassett, Local symmetry of plane curves, *Am. Math. Monthly* **92,** 1985, 689–707.
12. R. Kimmel and A. M. Bruckstein, Distance maps and weighted distance transforms, in *Proceedings, SPIE Geometric Methods in Computer Vision II, San Diego, California, July 1993,* Vol. 2031, pp. 259–268.
13. R. Kimmel and A. M. Bruckstein, Shape offsets via level sets, *CAD* **25**(5), March 1993, 154–162.
14. R. Kimmel, N. Kiryati, and A. M. Bruckstein, Distance maps and weighted distance transforms, *J. Math. Imaging Vision* (Special Issue on Topology and Geometry in Computer Vision), in press.
15. D. T. Lee, Medial axis transformation of a planar shape, *IEEE Trans. PAMI* **4,** 1982, 363–369.
16. F. Leymarie and M. D. Levine, Simulating the grassfire transform using an active contour model, *IEEE Trans. Pattern Anal. Machine Intell.* **14**(1), 1992, 56–75.
17. M. Leyton, Symmetry-curvature duality, *CVGIP: Graphic Models Image Process.* **38,** 1987, 327–341.
18. D. T. Lee, Medial axis transformation of a planar shape, *IEEE Trans. PAMI* **4,** 1982, 363–369.
19. F. Meyer, Skeletons in digital spaces, in *Image Analysis and Mathematical Morphology,* (J. Serra, Ed.), Vol. 2, Theoretical Advances, Academic Press, San Diego, 1988.
20. G. Matheron, Examples of topological properties of skeletons, in *Image Analysis and Mathematical Morphology,* Vol. 2, Theoretical Advances, (J. Serra, Ed.), Academic Press, San Diego, 1988.
21. U. Montanari, A method for obtaining skeletons using a quasi-Euclidean distance, *J. Assoc. Comput. Mach.* **15**(4), 1968, 600–624.
22. U. Montanari, Continuous skeletons from digitized images, *J. Assoc. Comput. Mach.* **16**(4), 1969, 534–549.
23. R. L. Ogniewicz, *Discrete Voronoi Skeletons,* Hartung-Gorre Verlag, Konstanz, 1993.
24. S. J. Osher and J. A. Sethian, Fronts propagating with curvature dependent speed: Algorithms based on Hamilton–Jacobi formulations. *J. Comput. Phys.* **79,** 1988, 12–49.
25. S. Riazanoff, B. Cervelle, and J. Chorowicz, Parametrisable skeletonization of binary and multi-level images, *Pattern Recognit. Lett.* **11,** January 1990, 25–33.
26. E. Rouy and A. Tourin, A viscosity solutions approach to shape-from-shading, *SIAM J. Numer. Anal.* **29**(3), June 1992, 867–884.
27. G. Sapiro and A. Tannenbaum, Affine invariant scale-space, *Int. J. Comp. Vision* **11**(1), 1993, 25–44.
28. J. A. Sethian, Curvature and the evolution of fronts, *Commun. Math. Phys.* **101,** 1985, 487–499.
29. J. A. Sethian and J. Strain, Crystal growth and dendritic solidification, *J. Comput. Phys.* **98,** 1992, 231–253.
30. D. Shaked and A. M. Bruckstein, *On Symmetry Axes and Boundary Curves,* CIS Report No. 9325, Computer Science Department, Technion, I.I.T., Haifa 32000, Israel, 1993.
31. M. Spivak, *A Comprehensive Introduction to Differential Geometry.* Publish or Perish, Berkeley, 1979.
32. K. Sugihara, Approximation of generalized Voronoi diagrams by ordinary Voronoi diagrams, *CVGIP: Graphical Models Image Process.* **55**(6), 1993, 522–531.
33. M. Sussman, P. Smereka, and S. J. Osher, *A Level Set Approach for Computing Solutions to Incompressible Two-Phase Flow,* Department of Math, UCLA, Los Angeles, CA 90024-1555, June 1993.
34. B. J. H. Verwer, L. J. Van Vliet, and P. W. Verbeek, Binary and gray-value skeletons: Metrics and algorithms, *Int. J. Pattern Recognit. Artif. Intell.* **7**(5), 1993, 1287–1308.